

Age of Information Analysis in Hyperledger Fabric Blockchain-enabled Monitoring Networks

Minsu Kim, Sungho Lee, Chanwon Park, and Jemin Lee

Department of Information and Communication Engineering (ICE)

Daegu Gyeongbuk Institute of Science and Technology (DGIST), Korea

Email: kms0603@dgist.ac.kr, seuho2003@dgist.ac.kr, pcw0311@dgist.ac.kr, jmnlee@dgist.ac.kr

Abstract—Age of information (AoI) is a recently proposed metric for quantifying data freshness in real-time status monitoring systems where timeliness is of importance. In this paper, we explore the data freshness in the Hyperledger Fabric Blockchain-enabled monitoring network (HeMN) by leveraging the AoI metric. In HeMN, status updates from sources are transmitted through an uplink and recorded in a Hyperledger Fabric (HLF) network. To provide a stochastic guarantee of data freshness, we derive a closed-form of AoI violation probability by considering the transmission latency and the consensus latency. Then, we validate our analytic results through the implemented HLF platform. We also investigate the effect of the target successful transmission probability (STP) on the AoI violation probability.

I. INTRODUCTION

Real-time status monitoring systems have been deployed worldwide for time-critical applications such as traffic management and pollution detection. These systems usually consist of a source and a destination. Specifically, the source generates a status update (or packet) with observed information and transmits it to the destination where status updates (or packets) are received and recorded. In such cases, decisions are made based on the observed information from the source, but outdated data may lead to incorrect decisions. Therefore, it is of importance for real-time status monitoring systems to provide fresh data, in order to prevent undesirable outputs. To quantify data freshness, AoI has been proposed in [1]. It is defined as the elapsed time from the generation of the latest received status updating packet.

The AoI has been analyzed for real-time IoT applications in order to capture the timeliness of monitoring data [2]–[4]. In [2], the optimal sampling policy is obtained to minimize the weighted sum-AoI in energy harvesting enabled IoT networks. In [3], the average AoI penalty function of an energy harvesting IoT system is obtained and the status update frequency is optimized to minimize the average AoI penalty function. An AoI-energy trade-off is studied for IoT monitoring systems and the average AoI is minimized by optimizing the transmission power of an IoT device in [4]. However, all of the previous papers did not consider the case when information is stored in a blockchain, which cannot guarantee data integrity.

Recently, a blockchain has been regarded as a promising decentralized data management platform for IoT devices aiming to eliminate the need for a central authority [5]–[7]. A blockchain integrated IoT platform is presented for real-time monitoring to provide data integrity [5]. In [6],

the communication cost of periodic updates is analyzed in Ethereum blockchain for lightweight IoT devices, which only store the head of blocks. For the blockchain-enabled wireless IoT network, the optimal deployment of the nodes for maximizing transaction throughput is investigated in [7]. However, data freshness in blockchain platforms is not analyzed in the previous papers [5]–[7], which fails to show the timeliness of stored data.

A blockchain may be selected as the underlying system of an alarm system (e.g., pollution or fire detection) in order to ensure data integrity. However, this system requires not only the integrity of monitored data but also the timeliness of it. If any of the two properties are not satisfied, the system may result in the wrong decision. Therefore, we analyze the data freshness in a Hyperledger Fabric (HLF) platform, which is one of the most utilized permissioned blockchain platforms. In HLF, the latest monitored information is stored in a distributed ledger with its history, which can provide data integrity.

In this paper, we investigate the data freshness in the Hyperledger Fabric Blockchain-enabled monitoring network (HeMN), where sources observe physical phenomena and update their status in a HLF network, which is connected at base stations (BSs). Sources and BSs are distributed randomly on the network, and each source transmits a packet to its nearest BS. To measure data freshness in HeMN, the AoI is utilized. We also analyze the AoI violation probability, which shows the probability that the target AoI is guaranteed. Our main contributions are as follows: 1) we derive the AoI violation probability in a closed-form by considering the consensus latency as well as the transmission latency, 2) we also obtain the experiment results by implementing the HLF platform v1.3 to verify analysis results, and 3) we explore the effect of the target successful transmission probability (STP) on the AoI violation probability of HeMN.

II. HLF TRANSACTION FLOW

In this section, we provide the overall structure of HLF and the components of the consensus process for a status update. In HLF, all changes made by transactions are committed to a distributed ledger. The ledger is a key-value database owned by peers in HLF, and transactions can update stored data with each corresponding key. Hence, all data is identified by each own key and a version number. In HLF, participants are all identified. Therefore, the costly consensus method in a public

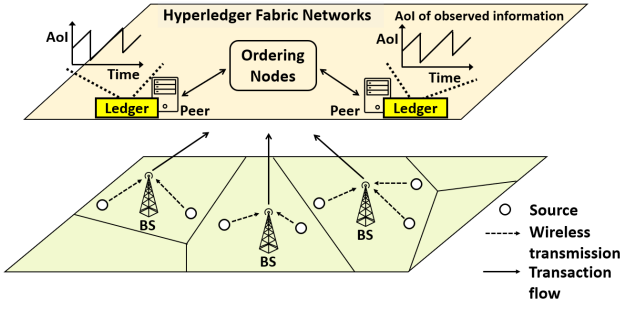


Fig. 1: An illustration of HeMN

blockchain, which is known as mining, is not necessary for HLF. Instead, the consensus process in HLF is composed of three phases: endorsing phase, ordering phase, and validation phase as described below. More detailed explanations on each phase are available in [8]

1) *Endorsing Phase*: The endorsing phase is to receive endorsements from the peers, which are entitled to simulate transactions against their own copied ledgers. The peers make sure that they have the exactly identical transaction simulation results. Then the transaction with the endorsements is transmitted to the ordering node.

2) *Ordering Phase*: The ordering phase is not only to arrange transactions in chronological order but also to generate new blocks with the ordered transactions. The ordering nodes continuously include transactions into a new block until it reaches the pre-defined maximum block size. To avoid high latency, a timer is prepared with the pre-defined timeout value. If the timer expires, the nodes instantly export the new block, regardless of the current number of transactions in the block.

3) *Validation Phase*: The validation phase is to validate newly delivered blocks to the peers. This phase consists of two sequential steps: verification and update. Firstly, the peers investigate if each transaction is properly endorsed according to the endorsement phase. Then, the peers check whether the key versions are identical to the ones currently stored in their copied ledgers. This verification is also called the multi-version concurrency check (MVCC) verification. Note that the key version increases each time the corresponding status is updated. In case the version numbers are different, the transaction is marked as invalid as well as become ineffective. Lastly, the peers update the status retained in their ledger.

III. HLF BLOCKCHAIN-ENABLED MONITORING NETWORK

A. System Model

We consider the HeMN composed of sources, BSs, and HLF network, where sources monitor physical phenomena (e.g., temperature or pollution level) and update the corresponding status stored in HLF as shown in Fig. 1. We assume the distribution of the sources follows a homogeneous Poisson Point Process (HPPP) Φ_s with spatial density λ_s . The source transmits a packet through a wireless uplink channel to the nearest BS. We assume that all the sources use the same transmission power P . The distribution of BSs also follows

a HPPP Φ_m with spatial density λ . Each channel is allocated to one source only in the cell of a BS to avoid the interference between the sources in the same cell.

We assume BSs are connected to HLF network, where the status information of sources are stored with their own key values. As shown in Fig. 1, a source monitors a physical phenomenon and generates a packet with newly observed information. The packet is delivered to HLF via a BS in a form of a transaction. Successfully received transactions can update their status information through the consensus process, which is described in Sec. II.

We define the consensus latency as the total time for the commitment of a transaction, which is the summation of the latencies in each phase in Sec. II. Then, the total latency of the k th packet can be defined as

$$Z_k = X_k + Y, \quad (1)$$

where X_k is the consensus latency of the k th packet and Y denotes the transmission latency, which is required for transmitting a packet from a source to its associated BS. The consensus latency $\{X_k, k \geq 1\}$ is assumed to be independent and identically distributed (i.i.d.). From empirical results of a constructed HLF platform, the consensus latency for the k th packet is modeled as a Gamma random variable, of which pdf is given by

$$f_{X_k}(x) = \frac{\beta^\alpha}{\Gamma(\alpha)} x^{\alpha-1} e^{-\beta x}, \quad (2)$$

where α is the shape parameter and β is the rate parameters. To determine the values of α and β for the consensus latency, we use the maximum likelihood estimation [9].

B. Analysis of Transmission Latency

In this subsection, we analyze the transmission latency Y of HeMN [10]. The signal to interference plus noise ratio (SINR) received by a BS at \mathbf{y}_0 from a source located at \mathbf{x}_0 under Rayleigh fading channel is given by

$$\text{SINR} = \frac{P h_{\mathbf{x}_0, \mathbf{y}_0} L_{\mathbf{x}_0, \mathbf{y}_0}^{-n}}{I + N_0 W}, \quad (3)$$

where $h_{\mathbf{x}_0, \mathbf{y}_0}$ is the fading channel gain, i.e., $h_{\mathbf{x}_0, \mathbf{y}_0} \sim \exp(1)$, N_0 is the noise power, W is the channel bandwidth, $L_{\mathbf{x}_0, \mathbf{y}_0}$ is the distance between the source at \mathbf{x}_0 and the associated BS at \mathbf{y}_0 , and n is the pathloss exponent. In (3), I is the interference from other sources that use the same uplink frequency band, given by

$$I = P \sum_{\mathbf{x} \in \Psi_u \setminus \mathbf{x}_0} h_{\mathbf{x}, \mathbf{y}_0} L_{\mathbf{x}, \mathbf{y}_0}^{-n}, \quad (4)$$

where Ψ_u denotes the set of locations of the sources which use the same frequency band with the source at \mathbf{x}_0 . For the data rate R , STP p_c is given by

$$p_c = \mathbb{P}[W \log_2(1 + \text{SINR}) \geq R]. \quad (5)$$

To guarantee a certain level of STP, we can set the target rate \bar{R} as

$$p_c = \mathbb{P}[W \log_2(1 + \text{SINR}) \geq \bar{R}] \geq \zeta, \quad (6)$$

where ζ is the target STP.

Using (6), we define the transmission latency Y as D/\bar{R} , where D [bits] is the packet size. Then \bar{R} can be obtained by

$$\bar{R} = \int_0^\infty \bar{R}(r) 2\lambda\pi r \exp(-\lambda\pi r^2) dr, \quad (7)$$

where $\bar{R}(r)$ is the target rate when the distance between the source and the BS is fixed to r , i.e., $L_{x_o, y_o} = r$. Note that the distribution of the distance from the source and the nearest BS follows a Rayleigh distribution. From the definition of SINR in (3), p_c can be given by

$$p_c = \exp\left(-\frac{r^n}{P} N_0 W \theta\right) \mathbb{E}_I \left[\exp\left(-\frac{r^n}{P} I \theta\right) \right], \quad (8)$$

where $\theta = 2^{\bar{R}(r)/W} - 1$ by using the cumulative distribution function (CDF) of the exponential random variable h_{x_o, y_o} . The dependence exists among the locations of interfering sources, so their distribution does not follow HPPP. Nevertheless, it is shown that this dependency can be weak [11], so we assume the distribution of the interfering sources follows the HPPP with spatial density λ . Note that a channel is allocated to one source only in the cell of a BS, so the density of uplink interfering sources is λ . According to [12, eq.3.21], Laplace transform of I can be given by

$$\mathcal{L}_I(s) = \exp\left\{-\lambda\pi s^{2/n} \frac{2\pi}{n \sin(2\pi/n)}\right\}. \quad (9)$$

From (9), p_c in (8) can be presented as

$$p_c = \exp\left(-\frac{r^n}{P} N_0 W \theta\right) \exp\left\{-\lambda\pi^2 \frac{2r^2\theta^{2/n}}{n \sin(2\pi/n)}\right\}. \quad (10)$$

To obtain a closed-form of $\bar{R}(r)$ from (6) and (10), we set $n = 4$ for tractability. We can then present $\bar{R}(r)$ as

$$\begin{aligned} \bar{R}(r) &= W \log_2 \left[1 + \left\{ \frac{P(-\pi^2\lambda + \sqrt{\pi^4\lambda^2 - 16N_0W \log \zeta})}{4N_0W r^2} \right\}^2 \right] \\ &= W \log_2 \left\{ 1 + \left(\frac{m}{r^2}\right)^2 \right\}, \end{aligned} \quad (11)$$

where m is:

$$m = \frac{P(-\pi^2\lambda + \sqrt{\pi^4\lambda^2 - 16N_0W \log \zeta})}{4N_0W}. \quad (12)$$

By substituting (11) with (7) and replacing r^2 with t , \bar{R} is given by

$$\begin{aligned} \bar{R} &= \lambda\pi W \int_0^\infty \log_2 \left\{ 1 + \left(\frac{m}{t}\right)^2 \right\} \exp(-\lambda\pi t) dt \\ &= \frac{\lambda\pi W}{\log 2} \int_0^\infty [\log \{t^2 + m^4\} - \log(t^2)] \exp(-\lambda\pi t) dt \\ &\stackrel{(a)}{=} \frac{W}{\log 2} \{ \log m - \text{Ci}(m\lambda\pi) \cos(m\lambda\pi) \\ &\quad - \text{Si}(m\lambda\pi) \sin(m\lambda\pi) + C + \log(\lambda\pi) \}, \end{aligned} \quad (13)$$

where (a) is obtained from [13, eq. 4.331, eq. 4.338]. $\text{Ci}(x)$ and $\text{Si}(x)$ are cosine integral and sine integral, respectively, and

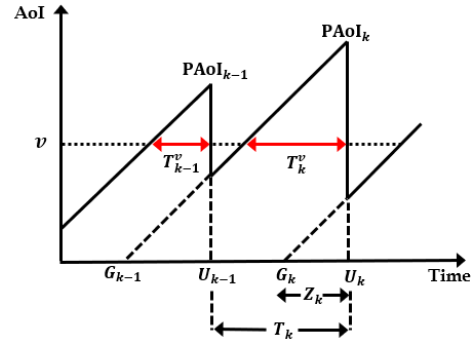


Fig. 2: A sample path of the AoI where G_k and U_k are the generation instant and update instant of the k th effective packet.

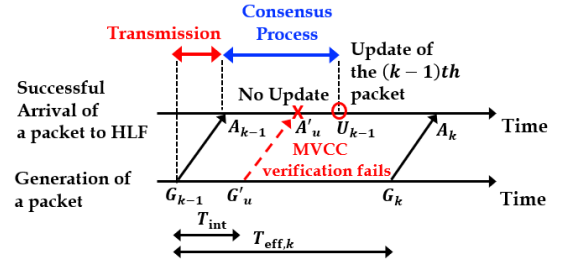


Fig. 3: The packet generated at G'_u is become invalid due to the MVCC verification.

C is an Euler constant. Using (13), the transmission latency Y is given by

$$Y = \frac{D \log 2}{W} \{ \log m - \text{Ci}(m\lambda\pi) \cos(m\lambda\pi) - \text{Si}(m\lambda\pi) \sin(m\lambda\pi) + C + \log(\lambda\pi) \}^{-1}. \quad (14)$$

Note that Y changes according to the target STP ζ .

IV. AOI ANALYSIS OF HEMN

In this section, we formulate the AoI violation probability for HeMN. As a metric for measuring the data freshness, the AoI is utilized. We focus on a specific status information, which is updated with a certain key value. We assume the source generates a packet with exponentially distributed inter-generation time with rate ρ_s . The inter-generation time of the two consecutive packets that successfully arrive at the BS from the source is denoted as T_{int} and we consider exponentially distributed T_{int} with rate $\rho = \rho_s p_c$. We assume the consensus latency X_k and T_{int} are independent.

As depicted in Fig. 3, not every generated packet can make a valid update because of the MVCC verification. We call the packets that make valid updates as *effective packets*. For the k th effective packet, we denote G_k as the generation instant at the source, A_k as the arrival instant at the BS, and U_k as the update instant for the ledger. In addition, G'_u and A'_u are for the generation and arrival instant of the u th invalid packet, respectively. Then, the inter-generation time of effective packets $T_{\text{eff},k}$ can be defined as $T_{\text{eff},k} = G_k - G_{k-1}$. The k th packet can be effective only if its arrival instant A_k is after U_{k-1} , which is the update instant of the previous $(k-1)$ th

$$\begin{aligned}
\mathbb{P}[\text{AoI} \geq v] &= \frac{\rho\beta^{2\alpha+1}}{(\beta+\rho\alpha)\Gamma(\alpha)^2} \sum_{n=0}^{\infty} \frac{(\rho-\beta)^n}{n!(\alpha+n)\rho^{\alpha+n+1}} \left[\frac{\Gamma(\alpha+n+1)}{\beta^\alpha} \gamma(\alpha, \beta T_c) - \sum_{k=0}^{\infty} \frac{(-1)^k (\rho T_c)^{\alpha+n+k+1}}{k!(\alpha+n+k+1)} B(\alpha+n+k+2, \alpha) \right. \\
&\quad \times T_c^\alpha {}_1F_1(\alpha; 2\alpha+n+k+2; -\beta T_c) \Big] + \frac{\rho}{(\beta+\rho\alpha)\Gamma(\alpha)} \left\{ \alpha \gamma(\alpha, \beta T_c) - \sum_{n=0}^{\infty} \frac{(-\beta T_c)^{2\alpha+n+1}}{n!\Gamma(\alpha)(\alpha+n+1)} B(\alpha+n+2, \alpha) \right. \\
&\quad \times {}_1F_1(\alpha; 2\alpha+n+2; -\beta T_c) - (\beta T_c)^{\alpha+1} B(\alpha, 2) T_c^\alpha {}_1F_1(\alpha; \alpha+2; -\beta T_c) \\
&\quad \left. + \sum_{n=0}^{\infty} \frac{(-\beta T_c)^{2\alpha+n+1}}{n!\Gamma(\alpha)(\alpha+n)} B(\alpha, \alpha+n+2) {}_1F_1(\alpha; 2\alpha+n+2; \beta T_c) \right\} + \frac{\Gamma(\alpha, \beta T_c)}{\Gamma(\alpha)}. \tag{19}
\end{aligned}$$

effective packet. Considering the transmission latency Y , any generated packet after $Z_{k-1} - Y$ can be an effective packet. Due to the memoryless property of T_{int} , $T_{\text{eff},k}$ can also be defined as

$$T_{\text{eff},k} = Z_{k-1} - Y + T_{\text{int}}, \tag{15}$$

The peak age of information (PAoI) is the AoI before the update instant [2]. For the k th effective packet, PAoI $_k$ is expressed as $T_{\text{eff},k} + Z_k$ as shown in Fig. 2. To see whether a certain level of freshness is guaranteed in HeMN, we can evaluate the AoI violation probability in HeMN based on the sample path analysis introduced in [14]. Then, the AoI violation probability is given by [14]

$$\mathbb{P}[\text{AoI} \geq v] = \frac{\mathbb{E}[T_k^v]}{\mathbb{E}[T_k]}, \tag{16}$$

where T_k^v is the time duration of the AoI being larger than the target AoI v between the update instants U_{k-1} and U_k , and T_k is the interval between update instants U_{k-1} and U_k . In HeMN, T_k^v can be defined as

$$\begin{aligned}
T_k^v &= \min \left\{ (\text{PAoI}_k - v)^+, T_k \right\} \\
&= \min \left\{ (X_{k-1} + X_k + T_{\text{int}} + Y - v)^+, X_k + T_{\text{int}} \right\}, \tag{17}
\end{aligned}$$

where $(\cdot)^+ = \max(0, \cdot)$. As shown in Fig. 2, T_k can be given by

$$T_k = T_{\text{eff},k} + Z_k - Z_{k-1} = X_k + T_{\text{int}}. \tag{18}$$

We now obtain the AoI violation probability of HeMN in the following theorem.

Theorem 1. *In HeMN, the AoI violation probability is given by (19) on the top of this page.*

Proof. In (16), the expectation of T_k^v is given by

$$\mathbb{E}[T_k^v] = \int_0^\infty \mathbb{P}[T_k^v \geq a] da. \tag{20}$$

Using (17) and (20), $\mathbb{E}[T_k^v]$ can be represented by

$$\begin{aligned}
\mathbb{E}[T_k^v] &= \int_0^{T_c} \int_0^\infty \mathbb{P}[(x + X_k + T_{\text{int}} - T_c) \geq a] f_{X_{k-1}}(x) dadx \\
&\quad + \int_{T_c}^\infty \int_0^\infty \mathbb{P}[X_k + T_{\text{int}} \geq a] f_{X_{k-1}}(x) dadx, \tag{21}
\end{aligned}$$

where $f_{X_{k-1}}(x)$ is in (2), and $T_c = v - Y$. In (21), $\mathbb{P}[(x + X_k + T_{\text{int}} - T_c) \geq a]$ can be given by

$$\begin{aligned}
&\mathbb{P}[T_{\text{int}} \geq a + T_c - x - X_k] \\
&\stackrel{(a)}{=} \int_0^{a+T_c-x} e^{-\rho(a+T_c-x-w)} f_{X_k}(w) dw + \int_{a+T_c-x}^\infty f_{X_k}(w) dw \\
&\stackrel{(b)}{=} \frac{\beta^\alpha e^{-\rho(a+T_c-x)} \gamma(\alpha, (\beta-\rho)(a+T_c-x))}{\Gamma(\alpha)} + \frac{\Gamma(\alpha, \beta(a+T_c-x))}{\Gamma(\alpha)}, \tag{22}
\end{aligned}$$

where (a) is obtained from the fact that $\mathbb{P}[T_{\text{int}} \geq a + T_c - x - X_k]$ is always one when X_k is larger than $a + T_c - x$, and the exponential distribution of T_{int} . In (22), $\gamma(\cdot, \cdot)$ and $\Gamma(\cdot, \cdot)$ are the incomplete gamma functions, given by

$$\gamma(\alpha, x) = \int_0^x t^{\alpha-1} e^{-t} dt, \quad \Gamma(\alpha, x) = \int_x^\infty t^{\alpha-1} e^{-t} dt. \tag{23}$$

Using (22), the inner integral of the first term in (21) can be obtained as

$$\begin{aligned}
&\int_0^\infty \mathbb{P}[(x + X_k + T_{\text{int}} - T_c) \geq a] da \\
&= \int_0^\infty \left[\frac{\beta^\alpha e^{-\rho(a+T_c-x)} \gamma(\alpha, (\beta-\rho)(a+T_c-x))}{\Gamma(\alpha)} \frac{\Gamma(\alpha, \beta(a+T_c-x))}{(\beta-\rho)^\alpha} \right. \\
&\quad \left. + \frac{\Gamma(\alpha, \beta(a+T_c-x))}{\Gamma(\alpha)} \right] da \\
&\stackrel{(a)}{=} \frac{\beta^\alpha}{\Gamma(\alpha)} \sum_{n=0}^{\infty} \frac{(\rho-\beta)^n}{n!(\alpha+n)} \int_0^\infty (a+T_c-x)^{\alpha+n} e^{-\rho(a+T_c-x)} da \\
&\quad + \frac{1}{\Gamma(\alpha)} \int_0^\infty \int_{\beta(a+T_c-x)}^\infty t^{\alpha-1} e^{-t} dt da \\
&= \underbrace{\frac{\beta^\alpha}{\Gamma(\alpha)} \sum_{n=0}^{\infty} \frac{(\rho-\beta)^n}{n!(\alpha+n)} \frac{\Gamma(\alpha+n+1, \rho(T_c-x))}{\rho^{\alpha+n+1}}}_{f_1(x)} \\
&\quad + \underbrace{\frac{\Gamma(\alpha+1, \beta(T_c-x))}{\beta\Gamma(\alpha)}}_{f_2(x)} + \underbrace{\frac{(x-T_c)}{\Gamma(\alpha)} \Gamma(\alpha, \beta(T_c-x))}_{f_3(x)}, \tag{24}
\end{aligned}$$

where (a) is from the fact that $\gamma(\alpha, x)$ can be represented as [13, eq. 8.354-1]

$$\gamma(\alpha, x) = \sum_{n=0}^{\infty} \frac{(-1)^n x^{\alpha+n}}{n!(\alpha+n)}. \tag{25}$$

Using (24), the first term in (21) can be represented as

$$\int_0^{T_c} \{f_1(x) + f_2(x) + f_3(x)\} f_{X_{k-1}}(x) dx, \quad (26)$$

where $f_i(x), i = 1, 2, 3$ is represented in (24). In (26), the first term can be given by

$$\begin{aligned} & \int_0^{T_c} f_1(x) f_{X_{k-1}}(x) dx \\ & \stackrel{(a)}{=} \frac{\beta^{2\alpha}}{\Gamma(\alpha)^2} \sum_{n=0}^{\infty} \frac{(\rho - \beta)^n}{n! (\alpha + n) \rho^{\alpha+n+1}} \int_0^{T_c} \left[\Gamma(\alpha + n + 1) \right. \\ & \quad \left. - \sum_{k=0}^{\infty} \frac{(-1)^k \{\rho(T_c - x)\}^{\alpha+n+k+1}}{k! (\alpha + n + k + 1)} \right] x^{\alpha-1} e^{-\beta x} dx \\ & \stackrel{(b)}{=} \frac{\beta^{2\alpha}}{\Gamma(\alpha)^2} \sum_{n=0}^{\infty} \frac{(\rho - \beta)^n}{n! (\alpha + n) \rho^{\alpha+n+1}} \left[\frac{\Gamma(\alpha + n + 1)}{\beta^\alpha} \gamma(\alpha, \beta T_c) \right. \\ & \quad \left. - \sum_{k=0}^{\infty} \frac{(-1)^k (\rho T_c)^{\alpha+n+k+1}}{k! (\alpha + n + k + 1)} T_c^\alpha B(\alpha + n + k + 2, \alpha) \right. \\ & \quad \left. \times {}_1F_1(\alpha; 2\alpha + n + k + 2; \beta T_c) \right], \quad (27) \end{aligned}$$

where $B(\cdot, \cdot)$ is the beta function and ${}_1F_1(\cdot; \cdot; \cdot)$ is the confluent hypergeometric function. The derivation of (a) is obtained since $\Gamma(\alpha, x) = \Gamma(\alpha) - \gamma(\alpha, x)$ and (b) is from [13, eq. 3.383-1]. Similarly, in (26), the second term can be represented by

$$\begin{aligned} & \int_0^{T_c} f_2(x) f_{X_{k-1}}(x) dx \\ & = \frac{\beta^{2\alpha}}{\Gamma(\alpha)^2} \int_0^{T_c} \left[\Gamma(\alpha + 1) - \sum_{n=0}^{\infty} \frac{(-\beta)^n (T_c - x)^{\alpha+n+1}}{n! (\alpha + n + 1)} \right] x^{\alpha-1} e^{-\beta x} dx \\ & = \frac{\alpha \gamma(\alpha, \beta T_c)}{\beta \Gamma(\alpha)} - \frac{T_c}{\Gamma(\alpha)^2} \sum_{n=0}^{\infty} \frac{(-1)^n (\beta T_c)^{2\alpha+n}}{n! (\alpha + n + 1)} \\ & \quad \times B(\alpha + n + 2, \alpha) {}_1F_1(\alpha; 2\alpha + n + 2; -\beta T_c). \quad (28) \end{aligned}$$

The third term in (26) is given by

$$\begin{aligned} & \int_0^{T_c} f_3(x) f_{X_{k-1}}(x) dx \\ & \stackrel{(a)}{=} -\frac{\beta^\alpha}{\Gamma(\alpha)^2} \int_0^{T_c} k \Gamma(\alpha, \beta k) (T_c - k)^{\alpha-1} e^{-\beta(T_c - k)} dk \\ & \stackrel{(b)}{=} -\frac{\beta^\alpha}{\Gamma(\alpha)^2} \int_0^{T_c} \left\{ \Gamma(\alpha) - \sum_{n=0}^{\infty} \frac{(-1)^n (\beta k)^{\alpha+n}}{n! (\alpha + n)} \right\} \\ & \quad \times k (T_c - k)^{\alpha-1} e^{-\beta(T_c - k)} dk \\ & \stackrel{(c)}{=} -\frac{T_c (\beta T_c)^\alpha}{\Gamma(\alpha)} B(\alpha, 2) {}_1F_1(\alpha; \alpha + 2; -\beta T_c) \\ & \quad + \frac{T_c}{\Gamma(\alpha)^2} \sum_{n=0}^{\infty} \frac{(-1)^n (\beta T_c)^{2\alpha+n}}{n! (\alpha + n)} B(\alpha, \alpha + n + 2) \\ & \quad \times {}_1F_1(\alpha; 2\alpha + n + 2; -\beta T_c), \quad (29) \end{aligned}$$

where (a) is obtained by substituting k for $T_c - x$, (b) is from (25) and (c) is obtained by the similar steps used in (27) and

TABLE I: Estimated shape (α) and rate parameters (β) for a Gamma distribution

Target STP	Average estimate (α, β)	Target STP	Average estimate (α, β)
0.3	(5.64, 3.01)	0.7	(7.18, 3.73)
0.4	(5.94, 2.45)	0.8	(7.71, 4.12)
0.5	(5.39, 2.85)	0.9	(7.50, 4.35)
0.6	(5.42, 2.84)	1.0	(6.57, 3.82)

then simplified by using ${}_1F_1(a; b; z) = e^z {}_1F_1(b - a; b; -z)$ in [13, 9.212-1].

Now, we derive the second term of (21). In the integral range of a , $X_k + T_{\text{int}} \geq 0$ holds. Hence, we have

$$\begin{aligned} & \int_{T_c}^{\infty} \int_0^{\infty} \mathbb{P}[X_k + T_{\text{int}} \geq a] da f_{X_{k-1}}(x) dx \\ & \stackrel{(a)}{=} (\mathbb{E}[X_k] + \mathbb{E}[T_{\text{int}}]) \int_{T_c}^{\infty} f_{X_{k-1}}(x) dx \\ & \stackrel{(b)}{=} \left(\frac{\alpha}{\beta} + \frac{1}{\rho} \right) \frac{\Gamma(\alpha, \beta T_c)}{\Gamma(\alpha)}, \quad (30) \end{aligned}$$

where (a) is obtained since X_k and T_{int} are independent and (b) is from the fact that X_k and T_{int} are the Gamma and exponential random variable, respectively.

Finally, $\mathbb{E}[T_k^v]$ is the summation of (27), (28), (29), and (30). Note that the $\mathbb{E}[T_k] = \mathbb{E}[X_k + T_{\text{int}}] = \frac{\alpha}{\beta} + \frac{1}{\rho}$. Therefore, we obtain (19) by the ratio of $\mathbb{E}[T_k^v]$ and $\mathbb{E}[T_k]$ as (16) \square

Note that the AoI violation probability in Theorem 1 can be applied to general HLF networks with version 1.0 or higher ¹.

V. NUMERICAL RESULTS

In this section, we verify the AoI violation probability analysis and show the impact of ζ on it. We set $\rho_s = 15$, $P = 1$ W, $N_0 = -100$ dBm, $W = 1$ MHz, $D = 500$ Kb, and $\lambda = 0.0001$ (BS/km²) as default values. We implement experiments for data freshness analysis in a HLF platform v1.3 on one physical machine with Intel(R) Xeon W-2155 @ 3.30GHz. We generate the transactions with exponentially distributed inter-generation time to update a certain target key-value, which takes 30 percent of the whole generation. We also measure the consensus latency of the generated target transactions for different ζ from 0.3 to 1. Then, we fit statistical distribution for the thousand samples at different ζ . The corresponding estimated parameters are averaged over five runs and shown in Table I

In Figure 4, we compare the analysis results with the simulation and experiment results as a function of v at different ζ . In the simulations, the sample path of the AoI for the target key-value is generated and iterated over 10000 times in MATLAB environment. Fig. 4 shows that the analysis results match the experiment results obtained from the HLF platform. Hence, the assumption that the consensus latency follows a Gamma distribution is reasonable. Each AoI violation probability shows the different decay rates because the estimated

¹HLF with version 1.0 or higher includes the MVCC verification

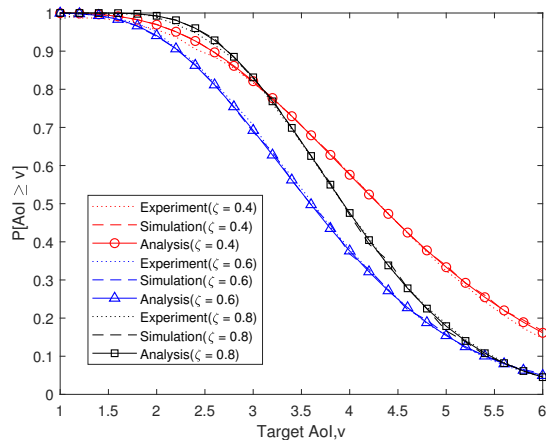


Fig. 4: AoI violation probability $\mathbb{P}[\text{AoI} \geq v]$ as a function of a target AoI v for different target STPs ζ .

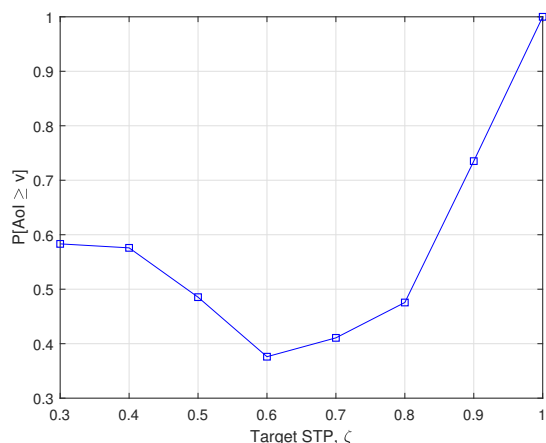


Fig. 5: AoI violation probability versus target STP ζ for the target AoI $v = 4$.

parameters and ζ are different. It can be seen that the AoI violation probability at $\zeta = 0.8$ is larger than the one at $\zeta = 0.4$ for low v . However, the result at $\zeta = 0.8$ shows the lowest AoI violation probability for high target AoI. Since the skewness of a Gamma distribution becomes reduced as the shape parameter increases, the mass of the distribution of consensus latency for $\zeta = 0.8$ tends to be concentrated on more right direction than others. Therefore, the result of $\zeta = 0.8$ shows the steepest decay rate for increasing v . Data freshness in HeMN can be more reliably guaranteed as v increases for higher ζ .

Figure 5 shows the AoI violation probability for different values of the target STPs with $v = 4$. We compute the AoI violation probabilities at each ζ from the empirical samples. As can be seen in Fig. 5, ζ and the AoI violation probability have a trade-off relation. In specific, when ζ is small, the AoI violation probability also becomes small due to the frequent outages of packets. As ζ increases, the AoI violation probability decreases. Since ζ can guarantee a certain level of STP, its increment results in more successfully received packets for the status update. However, after a certain point of ζ , both ζ and the AoI violation probability increase. This is from the

fact that large ζ not only guarantees a reliable transmission but also increases transmission latency. For this reason, it becomes difficult for the consensus process to be completed before the target AoI at high ζ . Hence, the optimal target STP ζ exists for minimizing the AoI violation probability.

VI. CONCLUSION

In this paper, we have provided the closed-form expression of the AoI violation probability in HeMN. Based on the sample path analysis, we analyze the characteristics of the AoI in HeMN by considering both the transmission latency and consensus latency. We validate our analysis results through the simulations and the experiments after constructing the HLF platform. The results show that our analysis results can provide the stochastic guarantee for data freshness in HeMN. Moreover, we show that the target STP and AoI violation probability have a trade-off relation and high target STP does not always guarantee data freshness. The AoI violation probability analysis for HeMN can be applied to AoI sensitive applications such as temperature monitoring systems or traffic management for vehicle systems, where both fresh information and data integrity are necessary.

REFERENCES

- [1] S. Kaul, R. Yates, and M. Gruteser, "Real-time status: How often should one update?" in *Proc. IEEE Conf. on Computer Commun.*, Orlando, FL, USA, Mar. 2012, pp. 1–5.
- [2] M. A. Abd-Elmagid, N. Pappas, and H. S. Dhillon, "On the role of age of information in the internet of things," *IEEE Commun. Mag.*, vol. 57, no. 12, pp. 72–77, 2019.
- [3] X. Zheng, S. Zhou, Z. Jiang, and Z. Niu, "Closed-form analysis of non-linear age of information in status updates with an energy harvesting transmitter," *IEEE Trans. Wireless Commun.*, vol. 18, no. 8, pp. 4129–4142, 2019.
- [4] Y. Gu, H. Chen, Y. Zhou, Y. Li, and B. Vucetic, "Timely status update in internet of things monitoring systems: An age-energy tradeoff," *IEEE Internet Things J.*, vol. 6, no. 3, pp. 5324–5335, 2019.
- [5] L. Hang and D. Kim, "Design and implementation of an integrated IoT blockchain platform for sensing data integrity," *Sensors*, vol. 19, no. 10, p. 2228, 2019.
- [6] P. Danzi, A. E. Kalør, C. Stefanović, and P. Popovski, "Delay and communication tradeoffs for blockchain systems with lightweight IoT clients," *IEEE Internet Things J.*, vol. 6, no. 2, pp. 2354–2365, 2019.
- [7] Y. Sun, L. Zhang, G. Feng, B. Yang, B. Cao, and M. A. Imran, "Blockchain-enabled wireless internet of things: Performance analysis and optimal communication node deployment," *IEEE Internet Things J.*, vol. 6, no. 3, pp. 5791–5802, 2019.
- [8] S. Lee, M. Kim, J. Lee, R.-H. Hsu, and T. Q. S. Quek, "Is blockchain suitable for data freshness? – age-of-information perspective," *arXiv preprint arXiv:2006.02735*, 2020.
- [9] H. C. Thom, "A note on the gamma distribution," *Monthly Weather Review*, vol. 86, no. 4, pp. 117–122, 1958.
- [10] C. Park and J. Lee, "Mobile edge computing-enabled heterogeneous networks," *arXiv preprint arXiv:1804.07756*, 2018.
- [11] T. D. Novlan, H. S. Dhillon, and J. G. Andrews, "Analytical modeling of uplink cellular networks," *IEEE Trans. Wireless Commun.*, vol. 12, no. 6, pp. 2669–2679, 2013.
- [12] M. Haenggi and R. K. Ganti, *Interference in large wireless networks*. Now Publishers Inc, 2009.
- [13] I. S. Gradshteyn and I. M. Ryzhik, *Table of integrals, series, and products*. Academic press, 2014.
- [14] J. P. Champati, H. Al-Zubaidy, and J. Gross, "On the distribution of age of information for the GI/GI/1/1 and GI/GI/1/2* systems: Exact expressions and bounds," in *Proc. IEEE Conf. on Computer Commun.*, Paris, France, Apr. 2019, pp. 37–45.